Review of Scientific Instruments

RESEARCH ARTICLE | AUGUST 13 2024

Visible core spectroscopy at Wendelstein 7-X

Special Collection: Proceedings of the 25th Topical Conference on High-Temperature Plasma Diagnostics

O. P. Ford ; A. Langenberg ; T. Romba ; P. Pölöskei ; M. Zanini; S. Bannmann ; T. Gonda ; K. Ida ; R. Lopez Cansino ; N. Pablant ; J. de la Riva Villen ; C. Swee ; M. Yoshinuma ; A. Alonso ; B. Geiger ; V. Perseo ; E. Viezzer; W7-X Team

Rev. Sci. Instrum. 95, 083526 (2024)
https://doi.org/10.1063/5.0219469

AIP Publishing

Review of Scientific Instruments ARTICLE pubs.aip.org/aip/rsi

Visible core spectroscopy at Wendelstein 7-X

Cite as: Rev. Sci. Instrum. 95, 083526 (2024); doi: 10.1063/5.0219469
Submitted: 17 May 2024 • Accepted: 13 July 2024 •
Published Online: 13 August 2024

O. P. Ford,[1,a)] A. Langenberg,[1] T. Romba,[1] P. Pölöskei,[1] M. Zanini,[1] S. Bannmann,[1] T. Gonda,[2] K. Ida,[3] R. Lopez Cansino,[4] N. Pablant,[5] J. de la Riva Villen,[6] C. Swee,[7] M. Yoshinuma,[3] A. Alonso,[6] B. Geiger,[7] V. Perseo,[1] E. Viezzer,[4] and W7-X Team[b)]

AFFILIATIONS

[1] Max-Planck Institut für Plasmaphysik, 17491 Greifswald, Germany
[2] Auburn University, Auburn, Alabama 36849, USA
[3] National Institute for Fusion Science, Toki 509-5292, Japan
[4] Department of Atomic, Molecular, and Nuclear Physics, University Seville, Seville, Spain
[5] Princeton Plasma Physics Laboratory, Princeton, New Jersey 08543, USA
[6] Laboratorio Nacional de Fusión, CIEMAT, Av. Complutense 40, 28040 Madrid, Spain
[7] Department of Engineering Physics, University Wisconsin-Madison, Madison, Wisconsin 53706, USA

Note: This paper is part of the Special Topic on Proceedings of the 25th Topical Conference on High-Temperature Plasma Diagnostics.

[a)] **Author to whom correspondence should be addressed:** htpd24@oliford.co.uk

[b)] For the complete member list, please refer to T. Sunn Pedersen, Nucl. Fusion **62**, 042022 (2022).

ABSTRACT

This paper presents an overview of recent hardware extensions and data analysis developments to the Wendelstein 7-X visible core spectroscopy systems. These include upgrades to prepare the in-vessel components for long-pulse operation, nine additional spectrometers, a new line of sight array for passive spectroscopy, and a coherence imaging charge exchange spectroscopy diagnostic. Progress in data analysis includes ion temperatures and densities from multiple impurity species, a statistical comparison with x-ray crystal spectrometer measurements, neutral density measurements from thermal passive Balmer-alpha emission, and a Bayesian analysis of active hydrogen emission, which is able to infer electron density and main ion temperature profiles.

I. INTRODUCTION

The charge exchange recombination spectroscopy (CXRS) system of the Wendelstein 7-X (W7-X) stellarator was commissioned during the 2018 experimental campaign (OP1.2b). The overall design of the system and some initial results have been presented previously,[1] and for the subsequent campaign in 2022/3 (OP2.1), a number of extensions and upgrades were made to broaden the scope of the diagnostic. More advanced data analysis methods have also been developed, applicable to data from both the 2018 and 2023 campaigns.

The design of the in-vessel observation systems has not changed optically since originally reported, with each observation system consisting of a vacuum window, simple lenses, a fiber optic array, and also, in some cases, an aluminum mirror. However, the mechanical components have been upgraded to survive continuous 100 kW/m^2 plasma radiation, as required for W7-X long pulse operation.[2] Water-cooled copper-plated steel structures were installed surrounding the optics to reduce their exposure, and Spectrosil glass plates are installed in front of the vacuum windows to protect them from over-heating due to the x rays that constitute most of the plasma radiative heat load. Cooling of the pivoting shutters that contain the aluminum mirrors proved particularly challenging and was solved using multi-foil copper-straps (similar to the gas-puff imaging diagnostic[3]).

Figure 1 shows the schematic layout of the complete system, which is split in active spectroscopy (left), observing the neutral beam injection (NBI), and passive spectroscopy (right), which views the plasma on the opposite side of the stellarator. The active system was built with a large number of fibers (275) in the optical heads,

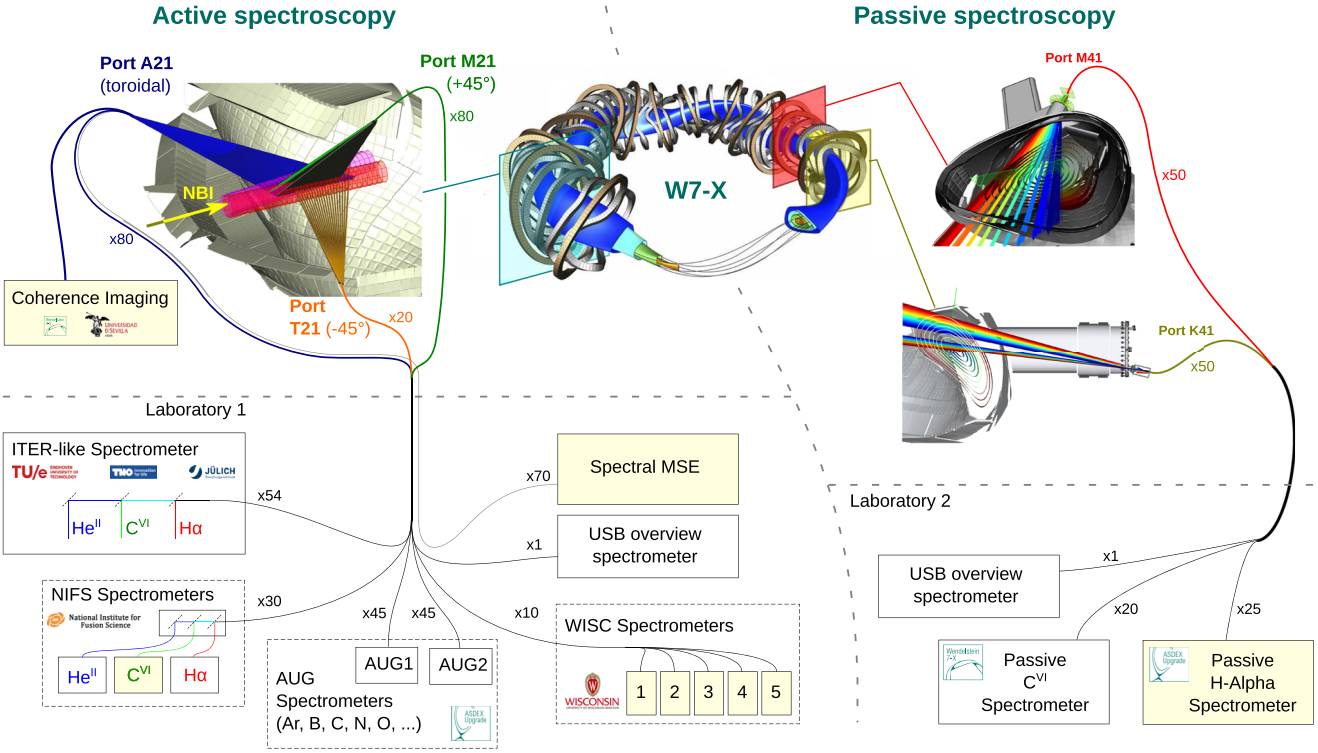

FIG. 1. Schematic layout of the W7-X CXRS system in the 2023 experimental campaign. (Left) 176 active spectroscopy lines of sight spread over three ports view the neutral beam injection and are connected to 13 spectrometers. (Right) 100 lines of sight over two optical systems are connected to three spectrometers for passive spectroscopy. The new spectrometers are shaded in yellow.

each corresponding to a particular line of sight. A selection of these are connected to a set of 100 m transfer fibers (176), which run to the spectroscopy laboratory, where a yet smaller number were connected to only three spectrometers. This under-subscription of available fibers in the original design was exploited in the last campaign by the addition of eight spectrometers, almost all through external collaborations. The passive spectroscopy system originally consisted of 50 lines of sight on the opposite side of the stellarator (yellow cross section) to which an additional 50 lines of sight have been added in the triangular cross section (red), where no divertor is present. One new spectrometer has been added to the passive spectroscopy system for hydrogen Balmer-alpha measurements.

II. ION TEMPERATURE

The C^{VI} channel of the ITER-like prototype spectrometer (ILS) continues to provide the primary ion temperature (T_i) measurements, which were critical for completing one of the main objectives of W7-X, confirming the neoclassical optimization.[4] Subtraction of the passive C^{VI} emission by interpolation of the signal before and after short periods of NBI operation (described previously[1]) is very reliable and now fully automated, but analysis of longer operation of NBI remains difficult and often requires manual attention, particularly in cases where strong accumulation of carbon takes place. Another 30 T_i measurements from the C^{VI} emission line were added without occupying additional observation channels by combining a third spectrometer with the existing pair provided by a collaboration with the National Institute for Fusion Science (NIFS). The light from 30 fibers is collimated, separated into three spectral channels by interference filters, and re-imaged onto three sets of fibers, each connected to one of the spectrometers. These additional data provide an improvement in spatial resolution, an important redundancy to the main T_i measurement in the case of software failures and confirmation that the instrumental effects of the two different spectrometers are correctly accounted for. The two variable wavelength spectrometers AUG1 and AUG2 (as they are constructed according to the ASDEX Upgrade CXRS spectrometer design[5]) are used to measure alternative impurity species, such as argon, nitrogen, or oxygen.

The same data acquisition software is used for each camera in all the spectrometers shown in Fig. 1. This software includes a processing module that fits a modified Gaussian function (see Ref. 1 for details) to the spectral lines. From the fitted width, the ion temperature is computed, including corrections for broadening due to the instrument function, fine-structure, and Zeeman effects. The latter two are provided by a web-service call to a general code capable of calculating the complete set of multiplet components for the hydrogen-like state of any low or medium charge atom.[6] The T_i profiles from the different species agree well when a sufficient concentration is present. To illustrate this, Fig. 2 shows the tem-

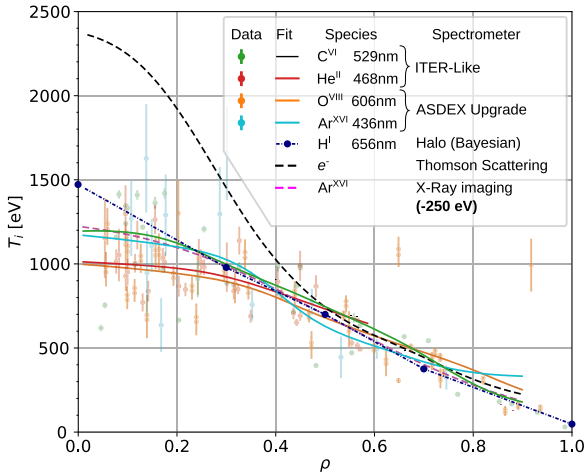

FIG. 2. Temperature profiles inferred from multiple species averaged over 14 20 ms NBI blips in discharge 20 181 016.027. Data points are shown with statistical error bars and fits are performed using a moving regression based on the Nadaraya–Watson kernel estimation with a fixed scale length of $\Delta\rho \approx 0.10$. The electron temperature profile fit determined from Thomson scattering data points normalized to the interferometer is indicated by the black dashed line. Inferred profiles are included from inversion of the x-ray imaging crystal spectrometer (magenta dashed line) and Bayesian analysis of beam halo balmer-alpha (blue dashed–dotted line, see Sec. IV).

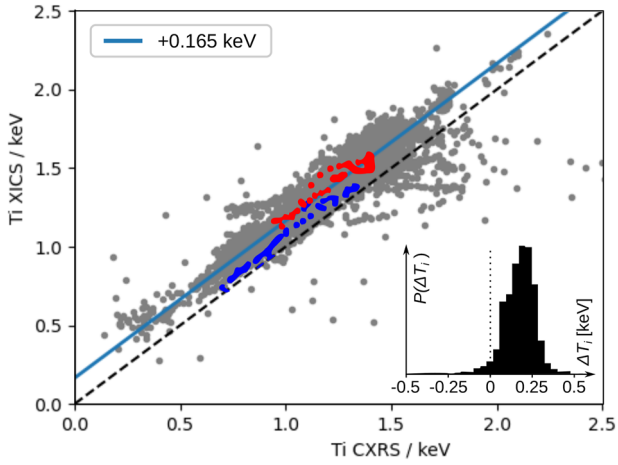

FIG. 3. Statistical comparison of ion temperature derived from the CXRS C^{VI} measurements and inversions of ion temperature from the x-ray imaging crystal spectrometer over the 2023 experimental campaign, showing an average offset of 165 eV. Data points from two individual shots are shown in red and blue. A histogram of the difference is shown as an inset.

perature profiles derived from the carbon (green), helium (red), and hydrogen (blue, see Sec. IV) measurements taken by using the ITER-like spectrometer as well as oxygen (orange) and argon (cyan) measurements derived from the ASDEX-Upgrade design spectrometers. The helium temperature is not corrected for the plume effect,[7] which may explain the apparent lower temperature in the core. The oxygen signal is weak due to the low concentration and contains two overlapping lines, n = 13–11 at 606.819 nm and n = 10–9 at 606.414 nm, which are fitted with a single temperature parameter. At $T_i = 1$ keV, the fine structure and Zeeman splitting corrections are around 10 eV for helium, 100 eV for carbon, 110 eV for oxygen, and 300 eV for the argon line. The fitted T_e profile from Thomson scattering are also shown for comparison, which is expected to agree with T_i in the outer region of plasma $r/a > 0.6$. Agreement to well within ±50 eV is seen between most spectrometers, and this is used a general estimation of the maximum systematic error expected on the main carbon T_i measurements.

Figure 2 also shows the inverted ion temperature profile from the x-ray imaging crystal spectrometer (XICS).[8] The data are averaged over 1.5 s, leading to vanishingly small statistical errors, which is also the case for the carbon CXRS measurements. Despite the small expected errors, an offset of −250 eV has to be applied to the XICS profile to obtain reasonable agreement with the CXRS results and the T_e in the outer half radius. An offset of approximately this magnitude is required to obtain good agreement in most discharges of the 2018 and 2023 experimental campaigns. Despite significant effort comparing different inversion methods and characterizing the XICS instrument function,[9] the cause of the systematic discrepancy remains unknown. Given that the same ionization state, Ar^{16+} is measured by CXRS and XICS, a physical difference in species temperatures is excluded. As there is good agreement of CXRS T_i with T_e in high collisionality plasmas, where power-balance shows that the T_e and T_i can differ by a maximum of 50 eV, the leading hypothesis is that an additional broadening mechanism is present in the XICS measurement. Figure 3 shows a statistical comparison of the two T_i measurements, averaged over the core region $r/a < 0.3$. An average offset of 165 eV is found, with 90% of the data falling in the range 0–300 eV. Individual plasma discharges with temporally varying ion temperature, such as those shown in red and blue in Fig. 3, exhibit an approximately constant offset. This suggests that a best-effort T_i profile with a systematic error of ±150 eV can be obtained from the XICS measurements by applying a constant offset that obtains the best agreement with T_e in the outer part of the plasma, or simply an offset of −165 eV if T_e is not available. This is particularly useful for discharges where CXRS measurements are not available (i.e., with no NBI blips). Efforts to isolate the systematic disagreement at W7-X and to make similar comparisons on other machines are on-going. These are of particular significance given that ITER will rely on x-ray spectroscopy measurements until the diagnostic neutral beam is available. An equivalent comparison has been made at the K-STAR tokamak[10] and shows agreement between the CXRS and x-ray spectroscopy to at least a similar level (± few 100 eV) for three individual discharges, although a statistical assessment of the disagreement has not been presented.

III. IMPURITY DENSITIES

All the spectrometers are intensity calibrated before and/or after each campaign for each optical array. For the variable wavelength spectrometers, this is done at multiple grating angles, so that a range of low- and medium-Z species can be measured.[11] Since the CXRS provides the only spatially localized measurements of the

low-Z species in the core plasma, these have been critical in confirming the strong turbulent impurity particle diffusion in ECRH-heated plasmas[12] and provided the first evidence of neoclassical-level impurity transport in NBI-heated discharges.[13]

A set of 18 larger 600 μm fibers were added to one optical head before the 2023 campaign, of which ten channels can be selected by five new high throughput spectrometers capable of measurements up to 10 kHz.[14] These spectrometers have so far been focused on impurity density measurements during laser-blow-off injection of high-Z impurities. The observation of Rydberg transitions excited by charge exchange from different ionization states are used to infer complete profiles of impurity particle diffusion and convection for high-Z species, definitively confirming high diffusion and an inward pinch in the core, beyond that predicted by neoclassical theory.[15]

IV. HYDROGEN BALMER-ALPHA SPECTROSCOPY

The ILS and NIFS spectrometers provide around 70 hydrogen Balmer-alpha (Hα) spectra along the beam. The spectra are a complex mix of around 14 Gaussian components, which can only be uniquely fit[1] for a few lines of sight where the Doppler shift of the beam emission components is sufficiently high. The spectral components have a non-linear dependence on a large number of partially known or unknown parameters including the plasma density, effective charge and ion temperature, the beam power, alignment, energy component composition and attenuation as well as the alignment, focal length and polarization sensitivity in each optical system. These dependencies make analysis complex but imply that a wealth of information is available from the spectra. In order to access it, a detailed forward model of the neutral beam source, plasma interation, and optical systems was developed.[16] This includes a full collisional-radiative model of the beam and coupled diffusion and collisional-radiative models of the neutral beam halo that surrounds the beam and is responsible for the majority of the thermal Balmer-alpha emissions. The model is used as part of a Bayesian analysis, simultaneously fitting all 50 spatial channels of the ILS Hα system. The results of the analysis provide the precise 3D neutral beam density distribution, which is required for the impurity density analysis and particle fueling. Other codes such as PyFIDASim[17] could be used for this purpose, but these rely on the nominal beam power and on the as-designed alignment parameters of the beam and optical system. In the Bayesian analysis, these parameters are inferred from the data, which revealed a 5 cm misalignment of the neutral beam system. Most importantly, the high fidelity of the beam and halo models allows profiles of electron density to be inferred, effectively giving a new diagnostic from existing hardware.[18] Although limited in spatial resolution, the profiles are entirely independent from the existing density profile information obtained from the interferometer normalized Thomson scattering diagnostic thereby provides an important cross-check of this critical quantity. Figure 4 (taken from Ref. 18) shows two example profiles, including one with a strong gradient at around mid-radius. Figure 2 shows the inferred ion temperature profile determined with this method for that discharge, using a five-point linear interpolation. Despite the complex dependence of the measurements on the physical parameters, the method is seen to give good quantitative agreement of the absolute values and to faithfully reproduce the shape of the profiles.

Each Hα spectrum also contains a small contribution from the charge exchange of beam and halo neutrals with fast ions, known as the FIDA signal (as typically deuterium is used). The FIDA signals from the ILS Hα spectrum were analyzed in detail,[19] revealing that in W7-X, it is dominated by charge exchange of fast ions with neutrals penetrating from the plasma edge. The active contribution is of greater interest, since it would provide one of the few measurements of fast-ion distribution near the plasma core, given that most diagnostics in the field measure fast-ion losses at walls. The 2023 campaign experiments were conducted with modulation of the neutral beams not directly observed, allowing isolation of the active FIDA signal.[20] Toward the end of the 2023 campaign, a new optical array and 25-channel spectrometer were added on the opposite side of W7-X to the NBI in order to continuously observe the passive Hα spectrum. In the future, this will be used to support the active systems via modeling and for information on the fast-ion population at the plasma edge.

V. PASSIVE SPECTROSCOPY

The passive core visible spectroscopy consists of two optical systems in different poloidal planes, connected to three spectrometers (see Fig. 1). In addition to the aforementioned FIDA studies,

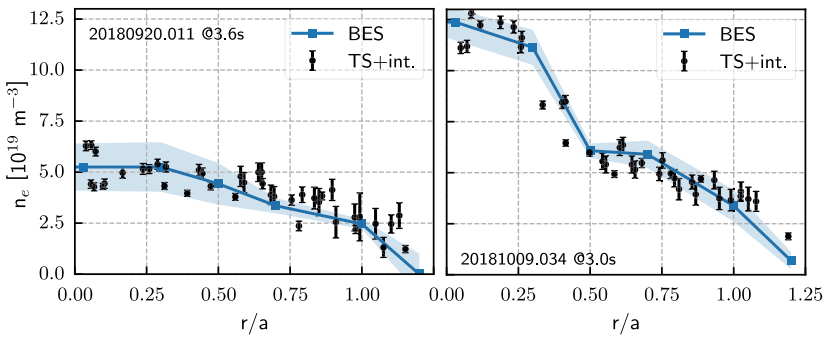

FIG. 4. Electron density profiles inferred by Bayesian analysis of active hydrogen Balmer-alpha data (blue), in comparison to the Thomson scattering profiles normalized to interferometry [Reprinted with permission from Bannmann *et al.* Plasma Phys. Controlled Fusion **66**, 065001 (2024) licensed under a Creative Commons Attribution (CC BY) license].

the passive Hα spectrometer is used to provide information on the neutral density inside the separatrix. Cold neutral hydrogen penetrating from the divertor and/or walls undergo successive charge exchange reactions with plasma ions, effectively giving a neutral that diffuses into the plasma before finally being ionized. This results in a neutral population that carries the local plasma temperature and falls approximately exponentially in density with decreasing plasma radius. The neutral density is determined by the intensity of a series of Gaussians of increasing Doppler broadening fit to the spectra.[21] Each temperature is related to a spatial position via the ion temperature profile measured by the active CXRS or XICS. The initial results give densities of similar order of magnitude to that expected from simple 1D neutral modeling[22] and EMC3-EIRENE simulations.[23] Although complex to analyze, the diagnostic provides the only information on neutral density inside the separatrix from recycling particles, which is critical for studies of particle transport.

A 20-channel spectrometer was added to provide regular measurements of the passive C^{VI} line at 529 nm created by charge exchange of C^{6+} with recycling neutrals and electron impact excitation of the local C^{5+} population. Despite the expected strong 3D variation of neutral density, the data are well described by a flux-surface constant emissivity and tomographic inversion of the emissivity profile has been used to study carbon transport inside the separatrix.[24] The emissivity profiles also enable calculation of the passive contribution to the active spectra for improved background subtraction. This has been applied successfully for a new video-based coherence imaging charge exchange recombination spectroscopy (CICERS) diagnostic,[25] which effectively measures a 2D image of the width of the C^{VI} line emission. The new system gives unprecedented spatial resolution and signal to noise ratio, but this comes at the cost of the spectral resolution required to isolate the passive signal. The tomography-based background subtraction method,[26] which relies on the passive C^{VI} spectrometer, is critical to the analysis of the images.

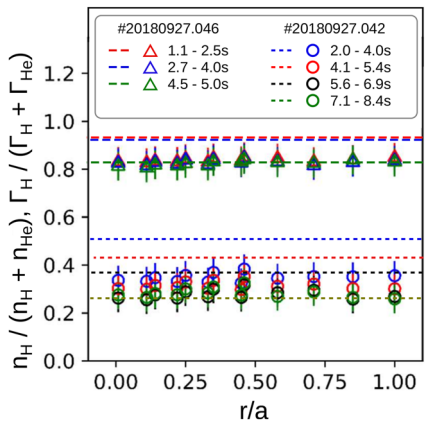

FIG. 5. Comparison of spatially resolved active measurements of hydrogen concentration $n_H/(n_H + n_{He})$ (points) compared to passive flux ratio measurements $\Gamma_H/(\Gamma_H + \Gamma_{He})$ in the scrape-off layer (dashed lines). Several time points of two discharges are shown for each. [Reprinted with permission from Beurskens *et al.*,[28] Nucl. Fusion **61**, 116072 (2021) licensed under a Creative Commons Attribution (CC BY) license].

Finally, a USB spectrometer covers the entire visible range for a single spatial channel. Gaussian fits are made automatically after each discharge to a large number of common bright visible lines, providing time traces of line intensity for many intrinsic and injected species. From the intensity ratio of the H^{I} and He^{II} lines at 486 and 468 nm, the flux ratio of $\Gamma_H/(\Gamma_H + \Gamma_{He})$ is derived using SXB coefficients under typical plasma conditions. Figure 5 shows this flux ratio (dashed lines) compared to the spatially resolved concentration $n_H/(n_H + n_{He})$ measurements made with the NIFS H and He spectrometers (triangles and circles). Since typical ECRH heated plasmas, such as these, exhibit flat concentration profiles, the flux ratio is in agreement with the average value to within ±0.2 or better and can be used as an operational proxy for the core hydrogen/helium concentration to this accuracy. The local concentration measurements shown in Fig. 5 are made using a relative intensity calibration method based on the measurements of reionization emission at the end of the discharge.[27]

VI. SUMMARY

The active and passive visible core spectroscopy systems at W7-X has been extended to provide spatially resolved information on many important plasma parameters for W7-X physics studies, including ion temperature; impurity densities; electron density; radial electric field and toroidal flow;[29] fast-ion distribution; and neutral hydrogen densities of the beam, halo, and recycling particles. Good agreement was found between ion temperature profiles from different species, giving an estimated error of ±50 eV for the main carbon based T_i profiles. A systematic offset of 165 ± 150 eV is found for x-ray spectroscopy measurements, suggesting an additional broadening mechanism. The ratio of helium and hydrogen line intensities on a passive USB spectrometer were found to provide a good estimation of central helium concentration in typical ECRH discharges to an accuracy of at least ±0.2.

ACKNOWLEDGMENTS

This work has been carried out within the framework of the EUROfusion Consortium, funded by the European Union via the Euratom Research and Training Programme (Grant Agreement No. 101052200—EUROfusion). Views and opinions expressed, however, are those of the author(s) only and do not necessarily reflect those of the European Union or the European Commission. Neither the European Union nor the European Commission can be held responsible for them.

AUTHOR DECLARATIONS

Conflict of Interest

The authors have no conflicts to disclose.

Author Contributions

O. P. Ford: Conceptualization (lead); Data curation (equal); Formal analysis (equal); Visualization (equal); Writing – original draft (lead). **A. Langenberg**: Data curation (equal); Investigation (equal); Visualization (equal). **T. Romba**: Conceptualization (lead);

Investigation (lead); Methodology (lead); Project administration (lead); Writing – original draft (lead); Writing – review & editing (lead). **P. Pölöskei**: Data curation (equal). **M. Zanini**: Data curation (equal). **S. Bannmann**: Data curation (equal); Formal analysis (equal); Investigation (equal); Methodology (equal); Software (equal). **T. Gonda**: Data curation (equal). **K. Ida**: Data curation (equal); Funding acquisition (equal); Methodology (equal). **R. Lopez Cansino**: Data curation (equal). **N. Pablant**: Data curation (equal); Validation (equal); Writing – review & editing (equal). **J. de la Riva Villen**: Data curation (equal). **C. Swee**: Data curation (equal); Methodology (equal). **M. Yoshinuma**: Data curation (equal). **A. Alonso**: Data curation (equal); Funding acquisition (equal); Methodology (equal); Software (equal). **B. Geiger**: Funding acquisition (equal); Project administration (equal). **V. Perseo**: Resources (equal); Supervision (equal). **E. Viezzer**: Funding acquisition (equal); Project administration (equal).

DATA AVAILABILITY

Raw data were generated at the Wendelstein 7-X large scale facility. Derived data supporting the findings of this study are available from the corresponding author upon reasonable request.

REFERENCES

[1] O. P. Ford *et al.*, "Charge exchange recombination spectroscopy at Wendelstein 7-X," Rev. Sci. Instrum. **91**, 023507 (2020).
[2] R. König *et al.*, "Diagnostics design for steady-state operation of the Wendelstein 7-X stellarator," Rev. Sci. Instrum. **81**, 10E133 (2010).
[3] J. Terry *et al.*, "The realization of a gas puff imaging system on the Wendelstein 7-X stellarator," Rev. Sci. Instrum. (submitted) (2024); arXiv:2405.09705.
[4] C. Beidler *et al.*, "Demonstration of reduced neoclassical energy transport in Wendelstein 7-X," Nature **596**, 221–226 (2021).
[5] E. Viezzer *et al.*, "High-resolution charge exchange measurements at ASDEX upgrade," Rev. Sci. Instrum. **83**, 103501 (2012).
[6] D. Gradic, M. Krychowiak, R. König, F. Henke, M. Otte, V. Perseo, T. S. Pedersen, and W.-X. Team, "Impurity temperatures measured via line shape analysis in the island scrape-off-layer of Wendelstein 7-X," Plasma Phys. Controlled Fusion **64**, 075010 (2022).
[7] A. Kappatou *et al.*, "A forward model for the helium plume effect and the interpretation of helium charge exchange measurements at ASDEX upgrade," Plasma Phys. Controlled Fusion **60**, 055006 (2018).
[8] A. Langenberg *et al.*, "Prospects of X-ray imaging spectrometers for impurity transport: Recent results from the stellarator Wendelstein 7-X (invited)," Rev. Sci. Instrum. **89**, 10G101 (2018).
[9] N. A. Pablant, A. Langenberg, J. A. Alonso, M. Bitter, S. A. Bozhenkov, O. P. Ford, K. W. Hill, J. Kring, O. Marchuck, J. Svensson, P. Traverso, T. Windisch, and Y. Yakusevitch, "Correction and verification of x-ray imaging crystal spectrometer analysis on Wendelstein 7-X through x-ray ray tracing," Rev. Sci. Instrum. **92**, 043530 (2021).
[10] S. G. Lee *et al.*, "Cross comparisons of X-ray imaging crystal spectrometer and charge exchange spectroscopy from KSTAR," Fusion Sci. Technol. **76**, 942–946 (2020).
[11] T. Romba, "Validation of the W7-X CXRS for impurity density profiles," M.S. thesis, Technische Universiteit Eindhoven, 2021, https://research.tue.nl/nl/studentTheses/validation-of-the-w7-x-cxrs-for-impurity-density-profiles.
[12] T. Romba *et al.*, "Evaluation and validation of radial impurity density profiles from CXRS using neutral beam modelling in W7-X," Plasma Phys. Controlled Fusion **65**, 075011 (2023).
[13] T. Romba *et al.*, "Suppression of anomalous impurity transport in NBI-heated W7-X plasmas," Nucl. Fusion **63**, 076023 (2023).
[14] C. Swee *et al.*, "Design of a new charge exchange recombination spectroscopy diagnostic for impurity transport experiments at Wendelstein 7-X," Rev. Sci. Instrum. **93**, 103523 (2022).
[15] C. Swee *et al.*, "Impurity transport study based on measurement of visible wavelength high-n charge exchange transitions at W7-X," Nucl. Fusion **64**(8), 086062 (2024).
[16] S. Bannmann *et al.*, "Fast forward modeling of neutral beam injection and halo formation including full Balmer-α emission prediction at W7-X," J. Instrum. **18**, P10029 (2023).
[17] C. Swee *et al.*, "Impurity transport studies at the HSX stellarator using active and passive CVI spectroscopy," Plasma Phys. Controlled Fusion **64**, 015008 (2021).
[18] S. Bannmann *et al.*, "Bayesian inference of electron density and ion temperature profiles from neutral beam and halo Balmer-α emission at Wendelstein 7-X," Plasma Phys. Controlled Fusion **66**, 065001 (2024).
[19] P. Z. Poloskei *et al.*, "Experimental characterization of the active and passive fast-ion H-alpha emission in W7-X using FIDASIM," Nucl. Fusion **64**, 026008 (2023).
[20] P. Poloskei *et al.*, "First direct fast-ion density measurements with FIDA spectroscopy in Wendelstein 7-X," in Proceedings of the 65th Meeting APS Division of Plasma Physics, Denver, CO, 2023.
[21] K. Fujii *et al.*, "Study of neutral hydrogen transport in LHD core plasmas based on high dynamic-range Balmer-α spectroscopy," Nucl. Fusion **55**, 063029 (2015).
[22] S. Bannmann *et al.*, "Particle transport in reduced turbulence neutral beam heated discharges at Wendelstein 7-X," Nucl. Fusion (to be published) (2024).
[23] V. R. Winters *et al.*, "EMC3-EIRENE simulation of first wall recycling fluxes in W7-X with relation to H-alpha measurements," Plasma Phys. Controlled Fusion **63**, 045016 (2021).
[24] L. Vanó, "Carbon content and transport investigations on Wendelstein 7-X with charge exchange recombination spectroscopy," Ph.D. thesis, Technische Universität Berlin, 2022, https://depositonce.tu-berlin.de/items/f56d13a8-ffa5-4d64-bb2a-67a446d8f80e.
[25] R. Lopez-Cansino *et al.*, "First measurements with a coherence imaging charge exchange recombination spectroscopy (CICERS) diagnostic at Wendelstein 7-X," Plasma Phys. Controlled Fusion **66**, 045012 (2024).
[26] R. Lopez-Cansino *et al.*, "2D core ion temperature and impurity density measurements with Coherence Imaging Charge Exchange Recombination Spectroscopy (CICERS) at Wendelstein 7-X," Rev. Sci. Instrum. (to be published) (2024).
[27] K. Ida *et al.*, "Measurement of radial profiles of density ratio of helium to hydrogen ion using charge exchange spectroscopy with two-wavelength spectrometer," Rev. Sci. Instrum. **86**, 123514 (2015).
[28] M. Beurskens *et al.*, "Ion temperature clamping in Wendelstein 7-X electron cyclotron heated plasmas," Nucl. Fusion **61**, 116072 (2021).
[29] J. Alonso *et al.*, "Plasma flow measurements based on charge exchange recombination spectroscopy in the Wendelstein 7-X stellarator," Nucl. Fusion **62**, 106005 (2022).